Preprint
UCRL-JC-137493

X-Ray Photoionized Plasmas in the Laboratory

R.F. Heeter, M.E. Foord, R.S. Thoe, J.A. Emig
P.T. Springer, J. Bailey, M. Cuneo, C. Deeney

This article was submitted to
Atomic Data Needs for X-Ray Astronomy Workshop
Greenbelt, MD, December 20, 1999

April 22, 2000

U.S. Department of Energy

Lawrence
Livermore
National
Laboratory

X-Ray Photoionized Plasmas in the Laboratory

R.F. Heeter, J.A. Emig, M.E. Foord, R.S. Thoe and P.T. Springer

Lawrence Livermore National Laboratory, PO Box 808, Livermore, CA 94551

J. Bailey, M. Cuneo, and C. Deeney

Sandia National Laboratories, PO Box 5800, Albuquerque, NM 87185

ABSTRACT

The advanced spectroscopic capabilities of the new X-ray telescopes Chandra and XMM lead to a need for improved benchmarking of models for the photoionized accretion-disk plasmas which represent over half of known astrophysical X-ray sources. We report the first laboratory experimental results using 120 TW, 180 eV Z-pinch plasmas to drive iron samples into the photoionized equilibrium. The pinch spectrum, temperature, power and uniformity have been characterized in order to qualify it as a photoionization driver. Preliminary time-integrated (8 Å to 18 Å) and time-resolved (12.5 Å to 16 Å) absorption and emission spectra of photoionized L-shell Fe and K-shell Na and F were observed using X-ray crystal spectrometers. Plans for upcoming experiments are also discussed.

1. Introduction

This paper presents the basic approach and first results of laboratory experiments developed to help resolve one of the important physics challenges arising in X-ray astronomy, and outlines the foreseeable progress which is expected in this area in the coming year. A large fraction of astrophysical X-ray sources are accretion-powered objects where an intense core X-ray source illuminates and photoionizes the surrounding gas. The Chandra and XMM observatories are capable of obtaining spectroscopic data with much higher resolution than previously possible in X-ray astronomy. However, the usefulness of excellent spectroscopic data depends greatly upon one's confidence in the basic atomic physics of the models with which the data is interpreted. Users of these data interpretation tools ought to be able to specify a set of plasma conditions, calculate the ionization balance and other properties of such a plasma, and get similar results from multiple codes. We present the results of such a comparison for four major photoionization equilibrium models in Section 2. Confidence in the models can be greatly increased if the model predictions are directly benchmarked against experimental data obtained in well diagnosed laboratory experiments under known plasma conditions; however, until recently the photoionization dominated equilibrium was inaccessible to laboratory experiments. In Sections 3 and 4 we describe how Z-pinch driven intense X-ray sources now enable laboratory astrophysics experiments in the photoionization regime. We report the first

results and future plans from such a project in Sections 5 and 6. In future publications we expect to present fully diagnosed experimental photoionization data with which to better benchmark the models and thereby improve the physics foundations for X-ray astronomy.

2. Comparison of Models for Photoionized Plasmas

The photoionization equilibrium in plasma physics arises when the dominant terms in the ionization balance equations are the processes of photoionization (absorbed photon ejects electron from ion) and recombination (electron recombines with ion and emits photon or excites another electron). This situation occurs when the ratio of the X-ray flux to the electron density is sufficiently high that collisional ionization processes are negligible relative to photoionization processes. We are particularly interested in the low density regime where 3-body recombination may also be neglected relative to 2-body recombination processes, such that

$$n_i \Gamma_{rad} \int_x^\infty S(E)\sigma_i(E)E^{-1}dE = n_e n_{i+1}\alpha_{i+1}. \quad (1)$$

On the left side, n_i is the density of a given ion species, Γ_{rad} is the total radiation flux, and the integral term uses the spectral shape $S(E)$ and the photoionization cross section $\sigma_i(E)$ to determine the photoionization rate coefficient. On the right side, n_e is the electron density, n_{i+1} is the density of the next ionization stage, and α_{i+1} is the recombination rate coefficient for that stage. One traditionally sets $\xi \equiv \frac{4\pi\Gamma_{rad}}{n_e}$ and it then follows from Equation 1 that the ionization balance $\frac{n_{i+1}}{n_i}$, and indeed much of the physics of these non-LTE photoionized plasmas, is determined solely by fundamental atomic physics data (σ,α) and ξ, the photoionization parameter (Tarter et al. 1969; Tarter & Salpeter 1969).

In order to assess which experiments might best benchmark the models used for photoionized plasmas, we obtained iron ionization balance predictions from four photoionization codes used in the astrophysical community at $\xi \approx 150$ erg cm/s. The results appear in Figure 1, and show disagreement: predictions for the dominant charge state range from Fe XIV to Fe XXIII. These results should be considered preliminary, and consequently the codes are not identified until we can formalize the comparison. However, it appears that users of these data analysis tools should expect considerable disagreement between them (either due to "pilot error" or differences in the physics) and that even simple ionization balance data would be useful in testing the models experimentally. We are actively collaborating with several photoionization modeling groups in this area.

3. Z Pinch X-Ray Sources for Photoionization

The production of strongly X-ray photoionized plasmas in the laboratory has only recently become possible, with the advent of intense Z-pinch X-ray sources. To achieve a given photoionization parameter ξ one needs to maximize the X-ray flux on a given sample, while minimizing the sample

density. The first consideration implies placing the sample as close as possible to the strongest possible X-ray source. The second consideration must be balanced against the need to obtain high quality absorption and emission signals, which require maximizing the product of density and scale length. To minimize the density one would like the largest possible sample, but the scale length is constrained by the characteristics of the X-ray source and the need to maintain the entire sample at roughly the same photoionization equilibrium.

The strongest laboratory X-ray source on Earth today is the Z Machine at Sandia National Laboratory, which routinely produces upwards of 100 TW (10^{21} ergs/s) by driving 18 MA of electrical current through cylindrical arrays of 100–400 fine wires. The array as a whole is some 20–70 mm in diameter and 10–20 mm tall to start with, and each wire is on the order of 10 microns in diameter, about a tenth the thickness of a human hair. The Lorentz force acting on the parallel currents causes the wire array to accelerate inwards, reaching velocities on the order of 100 km/s over some 100 ns. The convergence of the array results in stagnation on axis, at which time the kinetic energy of the imploding wires is converted into a 5–10 ns pulse of thermal X-rays with a characteristic temperature of 100–200 eV (1–2 million K) from a region with a typical diameter of 1–2 mm.

It is interesting to compare the X-ray fluxes achieved at Z with astrophysical sources. Foil samples may be placed as close as 15 or 16 mm from the center of the pinch. Working in cylindrical geometry one finds that a 100 TW, 1 cm long pinch produces an X-ray flux at the sample in excess of 3×10^{19} ergs/s/cm^2, which is comparable to the X-ray flux just 1500 km from a neutron star with a luminosity of 10^{37} ergs/s. The 100 ns run-in time of the pinch provides time for a foil to "blow down" to 10^{-4} or less of solid density, and enables Z to produce photoionization regimes with $\xi \sim 100$ erg cm/s, comparable to conditions found in such accretion powered astrophysical objects as X-ray binaries and active galactic nuclei. Some care must be taken with this comparison because the details of the photoionizing spectrum, plasma composition and plasma density are necessarily different. Nonetheless, the fundamental processes governing the photoionization equilibrium are the same. We therefore anticipate that benchmarking of the photoionization codes with Z-pinch data will enable astronomers to more accurately (or at least more confidently) use these models to interpret X-ray astronomy data.

4. Experimental Objectives and Concept

To properly benchmark the models, one must characterize the flux, spectrum (temperature) and uniformity of the pinch, photoionize a sample into an astrophysically interesting regime, and then measure the absorption and emission of the sample while simultaneously determining the sample density and temperature, preferably in a model independent way. The conceptual layout of such an experiment is shown in Figure 2. In this concept, the pinch is to be characterized using several Sandia diagnostics, which include time gated pinhole cameras, time resolved absolutely calibrated transmission grating spectrometers, calibrated X-ray diodes and bolometers, and a radially

and temporally resolved X-ray streak camera. The sample absorption and emission, as well as one band of the pinch spectrum, are to be measured with one or more curved crystal spectrometers, with the Z pinch used as a backlighter for the absorption measurement. The ratio of the absorption spectrum to the pinch spectrum then yields the opacity. The sample temperature is to be extracted from the slope of the recombination continuum as well as line ratios of low-Z tracers in the sample. The sample density is to be obtained by imaging the expansion of the foil with a time gated pinhole camera, using the known initial conditions of the foil.

Although reasonably straightforward in principle, this concept has a number of subtleties which require significant attention to be paid to the experimental design. For instance, in order to compare the time dependent experiment with time independent equilibrium models, the sample must have time to come into equilibrium with the radiation field of the pinch. One must then produce time gated measurements of the sample in the "steady state" regime, before the X-ray pulse from the pinch terminates. One would also like the sample to ionize and expand in a uniform manner, so that all parts of the sample are in the same equilibrium. One also needs the sample to be sufficiently opaque that an absorption spectrum may be obtained, and sufficiently massive that an emission spectrum may be obtained. Given the millimeter scale lengths available in a Z pinch, these considerations all tend towards higher density samples. This conflicts with the desire to minimize the sample density in order to eliminate 3-body processes and maximize the photoionization parameter. One must therefore take care in designing the experiment, to ensure that a balance may be found whereby all these objectives can be achieved simultaneously.

These experimental design issues have been addressed using 1-D and 2-D time dependent radiation hydrodynamics simulations with the LASNEX code (Zimmermann & Kruer 1975). The resulting sample is a foil composed of 200 Å of iron (the astrophysically interesting component) co-mixed with 300 Å of sodium fluoride (tracers to be used as temperature diagnostics). The foil is hydrodynamically tamped with 1000 Å of Lexan (C,H, and O) placed on either side, forming a sandwich configuration. The foil is 1 mm high and 0.5 mm wide, and placed face-on to the pinch to provide maximum uniformity of illumination. As shown in Figure 3, the run-in phase of the pinch allows the foil to blow down, and the 5–10 ns duration of the X-ray pulse is such that the foil conditions reach equilibrium from 2–4 ns following the peak of the X-ray pulse. (Here equilibrium conditions are defined as conditions whose values at a given time match the values expected in steady state for the same X-ray drive at that time.) This 2 ns time window poses one of the key challenges for the experiment: it forces the use of time gated rather than time integrated spectrometers to obtain the actual photoionization data, and is comparable to the timing jitter of the best available trigger signals on the machine. At the start of this 2 ns window, we calculate that the iron part of the foil will have expanded (in thickness) from 0.5 to 1200 microns. This maximizes ξ by bringing the foil density down as much as possible, and also allows the expansion of the foil to be imaged edge-on with a time gated pinhole camera. Based on 2-D (R-Z) calculations which account for the actual pinch geometry, we expect an electron density $n_e \sim 10^{19}/\mathrm{cm}^3$ and a mass density $\rho \approx 10^{-4}$ to $10^{-5}\mathrm{g}/\mathrm{cm}^3$, for ξ on the order of 10 to 100 erg cm/s. Under these conditions, preliminary

calculations suggest that the charge balance is insensitive to 3-body recombination effects and the low-density photoionization equilibrium described in Equation 1 is reached, although further modeling (with experimental data) is required to confirm this.

5. Initial Experiments and Results

Two preliminary photoionization experiments were carried out at Z in September 1999. The principal objectives of these two "shots" were to characterize in detail a particular pinch configuration and to validate the basic experimental design by obtaining as much foil data as possible. We used a 20 mm diameter tungsten wire array with 300 wires, each 10 μm in diameter. Tungsten was chosen because it has a line-free spectrum in the spectral range of interest (750–1300 eV, or roughly 8–16 Å), and the small (20 mm) many-wire pinch was chosen to provide the maximum X-ray flux onto the sample.

Figure 4 provides a view of the actual "target" (experiment). The wires of the array can be seen diverging out the top of the current return can, which is basically a cylinder with slots cut out to allow instruments to see through to the pinch. Two of the experimental foils can be seen: the first is face-on to the camera in the center of the picture, and the second is seen edge-on off to the right. Various graphite windows were used to limit the fields of view of various instruments. Graphite was chosen so that in the spectral range of interest only the foils and pinch would be visible. For the same reason, all pinch-facing high-Z surfaces were coated first with gold and then with boron. A schematic top view of the experiment is shown in Figure 5, which also details the various diagnostic instruments and their lines of sight.

The experimental results are as follows. In both shots (Z476 and Z477), the pinch produced 120 TW ($\pm$ 10%) of predominantly thermal X-rays with a characteristic temperature of 180 eV (Cuneo 1999). At the time of interest (2–4 ns after the peak X-ray power), radially resolved streak camera data gives a FWHM of 1.5 mm for the pinch diameter (Lazier 1999). Pinhole camera images of the X-ray emission above roughly 600 eV show adequate uniformity of the pinch at this time (Breeze 1999). A time integrated crystal spectrometer with spatial resolution along the pinch axis (vertical) direction obtained a high quality time integrated spectrum. This spectrum is shown in Figure 6, with tentative line identifications using a semi-empirical wavelength scale (Bailey 1999). The upper trace is a lineout taken through the top part of the foil, where no iron was deposited, and is simply the pinch spectrum with absorption from the Lexan part of the foil. The lower trace is a lineout taken through part of the foil containing the Fe:NaF mixture, and shows numerous lines from the sodium Lyman and Helium series, fluorine Lyman series, and both neon-like and fluorine-like iron (Fe XVII and Fe XVIII). Of particular interest is the Fe XVII 2p-nd series, with n ranging from 3 to at least 8. The iron spectral lines were identified based on recent data from the EBIT facility at LLNL (Brown et al. 1998; Brown 2000). One reason why the line identifications are only tentative is that the relative line strengths in photoionized plasmas are expected to be considerably different from those in collisional plasmas, which complicates the line identification

process, especially when one has only one or two spectra to analyze (Liedahl et al. 1990). The time integrated spectrum in Figure 6 is not ideal to benchmark photoionization models since over much of the integration period the foil was not expected to be in the photoionized regime, but it validates our ability to photoionize Fe into the L shell and produce highly ionized Na and F for spectral diagnostic use.

To obtain time resolved absorption and emission data we fielded a 3-crystal, 2-ns gated Johann curved crystal spectrometer belonging to LLNL. This spectrometer had not previously been used at Z, and a number of difficulties were encountered in this "shakedown" experiment, but we did obtain time gated data from 1-3 ns after the X-ray peak (a respectably close 1 ns from the desired "steady state" window), albeit with higher backgrounds than we would have liked. In these spectra we have tentatively identified lines belonging to Ne-like Fe XVII in absorption, along with the Lyman-α line of Fluorine, plus Fe XVII and Fe XVIII in emission. More importantly, we have identified solutions to the experimental difficulties and gained confidence that we can successfully field this instrument in our second generation experiments, which are scheduled for April or May 2000.

It was hoped that the sample density would be determined by imaging the expansion of the foil with a pinhole camera viewing the foil edge-on through a graphite window. However, we found that the field of view was contaminated by boron blowing back from the wall of the can and by carbon blowing off of the graphite walls, and with only two shots we were unable to properly tune the instrument filtering and gain settings in order to properly resolve the small amount of iron against these background sources. We have, however, identified two techniques to obtain the density measurement in future experiments. The first involves further tuning the pinhole camera, and the second involves placing the foil in a horizontal plane edge-on to the pinch, so that the foil expansion can be imaged spectroscopically in absorption with high signal. Other improvements to the experiments are also being developed.

6. Conclusions and Future Work

Photoionized plasmas are common in astrophysics, and detailed X-ray spectra of such plasmas are now being obtained by new missions such as Chandra and XMM. However, interpretation of these spectra rely on models which are difficult to bring into agreement. We have developed the first capability to produce near-steady-state, uniform photoionized plasmas in the laboratory, using foil samples placed near the Sandia Z Machine. In our first generation experiments the pinch appeared to work well as a photoionization driver, and we produced, as intended, L-shell iron, including a detailed time integrated absorption spectrum with Fe XVII and Fe XVIII, and time resolved absorption and emission spectra showing the same species with lower signal-to-noise. These first generation experiments were not expected to yield all of the data needed to benchmark the photoionization models. Based on these promising initial results, we are implementing various improvements in preparation for an upcoming second generation experiment scheduled for April/May 2000.

The authors especially thank T. Dimwoodie at Sandia for timing and data acquisition support. We also thank C. Coverdale, S. Breeze, D. Jobe, S. Lazier, J. McGurn, T. Nash and the Z Machine operations team at Sandia for experimental support, and the LLNL LDRD program for financial support. This work was performed under the auspices of the U.S. Department of Energy by University of California Lawrence Livermore National Laboratory under contract no. W-7405-Eng-48.

REFERENCES

Bailey, J. E. 1999, Private Communication

Breeze, S. 1999, Private Communication

Brown, G. V. 2000, PhD thesis, Auburn Univ.

Brown, G. V., Beiersdorfer, P., Liedahl, D. A., Widmann, K., & Kahn, S. M. 1998, Astrophysical Journal, 502, 1015

Cuneo, M. E. 1999, Private Communication

Lazier, S. E. 1999, Private Communication

Liedahl, D. A., Kahn, S. M., Osterheld, A. L., & Goldstein, W. H. 1990, Astrophysical Journal, 350, L37

Tarter, B. & Salpeter, E. E. 1969, Astrophysical Journal, 156, 953

Tarter, C. B., Tucker, W., & Salpeter, E. E. 1969, Astrophysical Journal, 156, 943

Zimmermann, G. B. & Kruer, W. L. 1975, Comments on Plasma Phys. and Cont. Fusion, 2, 85

Fig. 1.— Informal comparison of four photoionization codes at $\xi = 150$ erg cm/s.

Fig. 2.— Experimental Concept.

Fig. 3.— Simulated iron ionization (Z) and electron temperature (T_e) vs. time, with equivalent steady-state values shown.

Fig. 4.— Photo of first generation experimental target.

Fig. 5.— Schematic of first generation experiment.

Fig. 6.— Time integrated spectrum from a KAP convex crystal spectrometer.

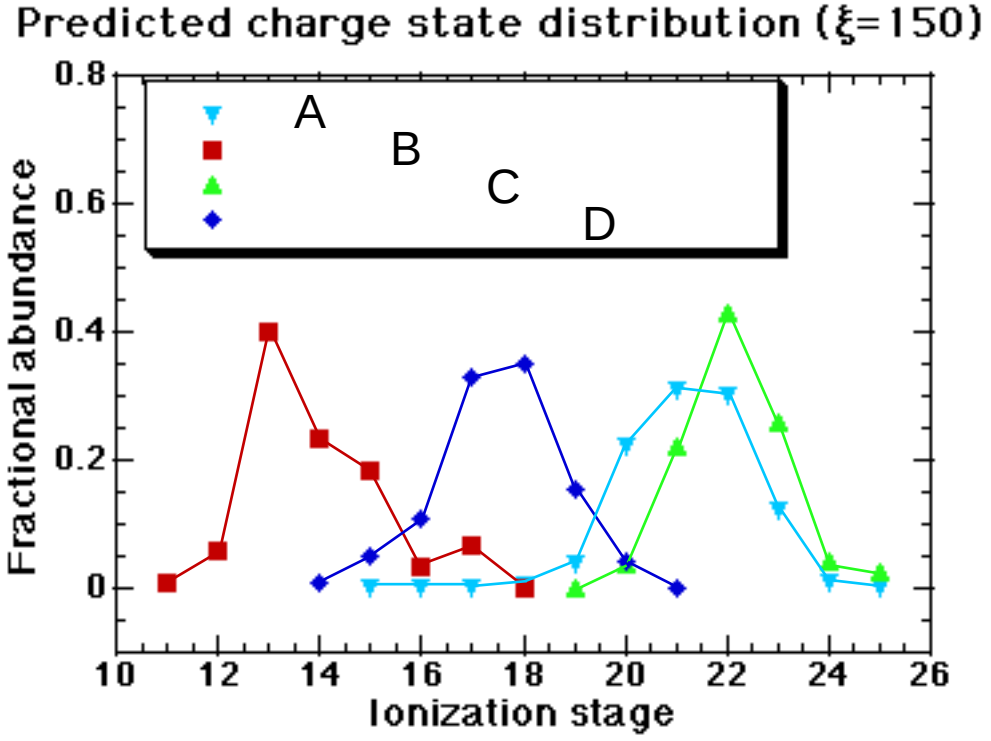
Predicted charge state distribution (ξ=150)
A
B
C
D
Fractional abundance
0.8
0.6
0.4
0.2
0
10
12
14
16
18
20
22
24
26
Ionization stage

Z-pinch photoionizes and backlights samples

Imaging curved crystal spectrometer

Absorption

Emission

Imaging curved crystal spectrometer

1-2 cm

Transmission grating spectrometer

w

l

w

$\rho = \frac{m_o}{Aw}$

Absorption Spectrum

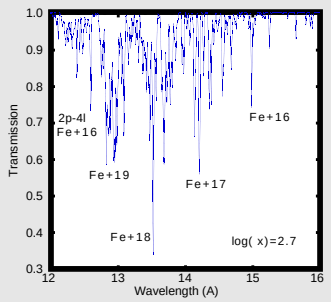

Z

X-ray Flux

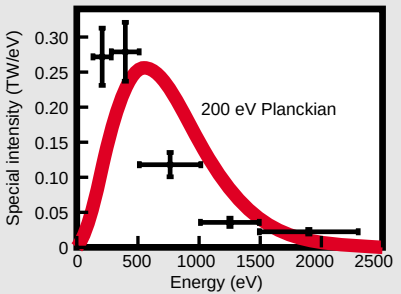

ξ

Emission Spectrum

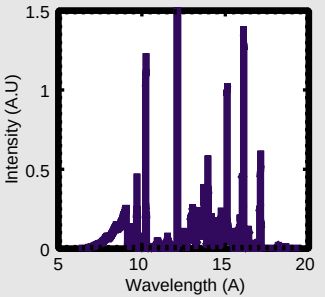

ρ, T_e, e_n, Z

Diagnostics measure densities, temperatures, Z, and ξ

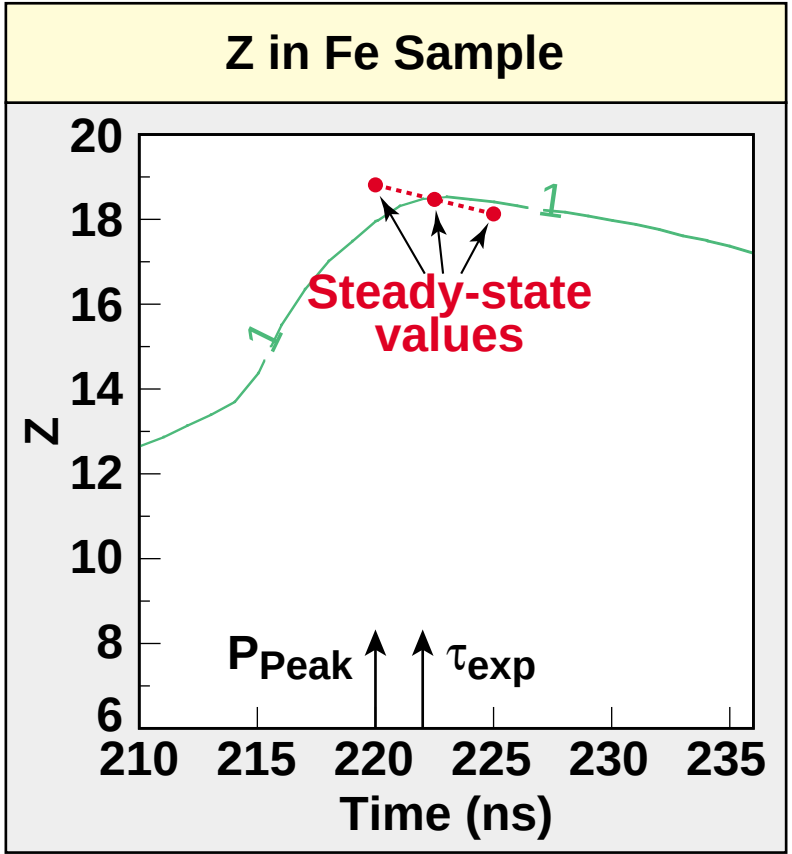
Z in Fe Sample
20
18
16
14
12
10
8
6
Z
Steady-state values
P_Peak
τ_exp
210
215
220
225
230
235
Time (ns)

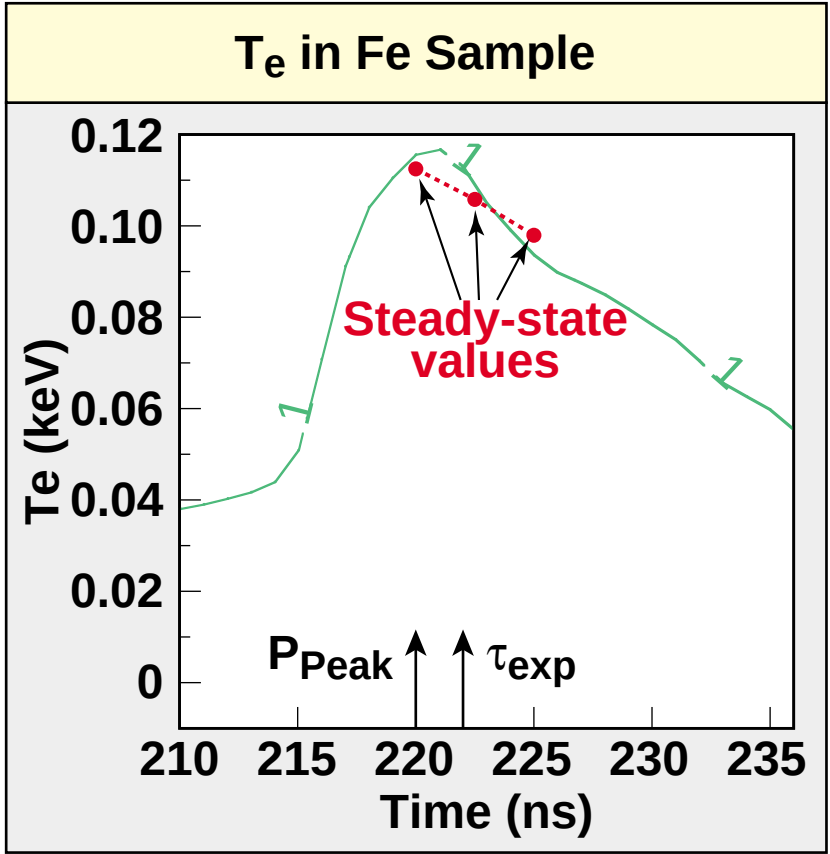
T_e in Fe Sample
0.12
0.10
0.08
0.06
0.04
0.02
0
Te (keV)
Steady-state values
P_Peak
τ_exp
210
215
220
225
230
235
Time (ns)

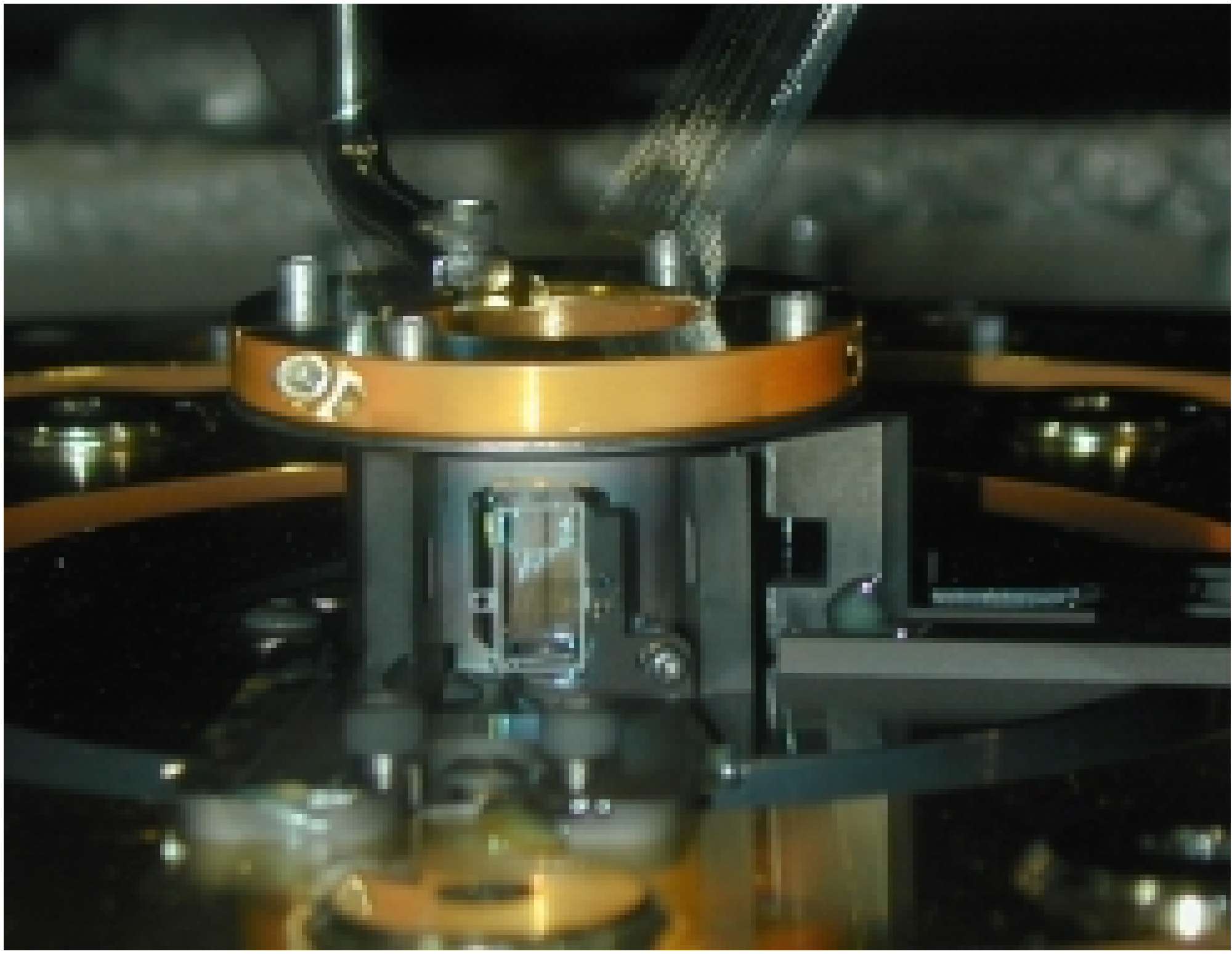

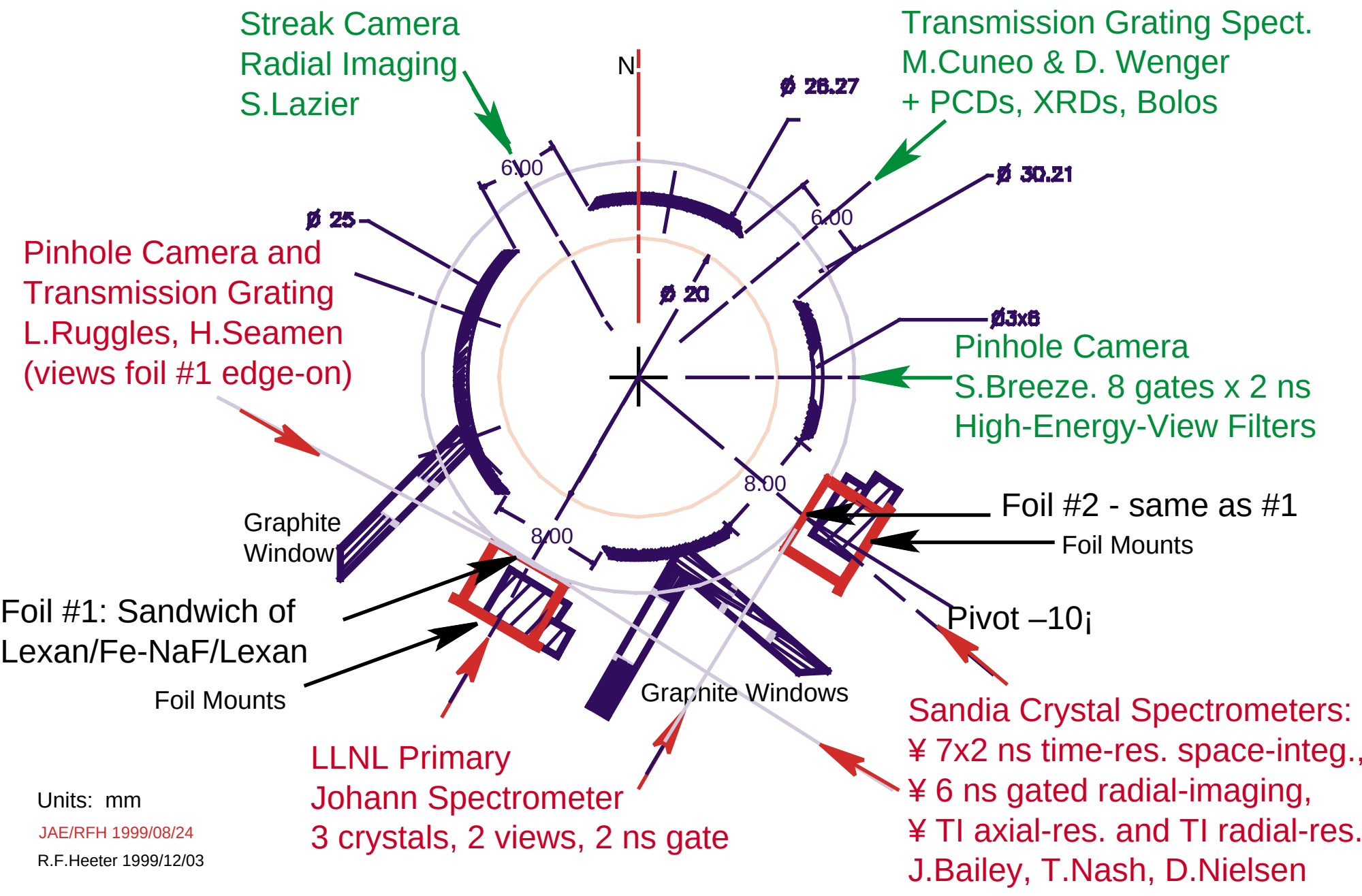
Streak Camera
Radial Imaging
S.Lazier
Transmission Grating Spect.
M.Cuneo & D. Wenger
+ PCDs, XRDs, Bolos
N
Ø 28.27
Ø 30.21
6.00
6.00
Ø 25
Ø 20
Pinhole Camera and
Transmission Grating
L.Ruggles, H.Seamen
(views foil #1 edge-on)
Ø3x6
Pinhole Camera
S.Breeze. 8 gates x 2 ns
High-Energy-View Filters
8.00
8.00
Graphite
Window
Foil #2 - same as #1
Foil Mounts
Foil #1: Sandwich of
Lexan/Fe-NaF/Lexan
Pivot –10¡
Foil Mounts
Graphite Windows
Sandia Crystal Spectrometers:
¥ 7x2 ns time-res. space-integ.,
¥ 6 ns gated radial-imaging,
¥ TI axial-res. and TI radial-res.
J.Bailey, T.Nash, D.Nielsen
LLNL Primary
Johann Spectrometer
3 crystals, 2 views, 2 ns gate
Units: mm
JAE/RFH 1999/08/24
R.F.Heeter 1999/12/03

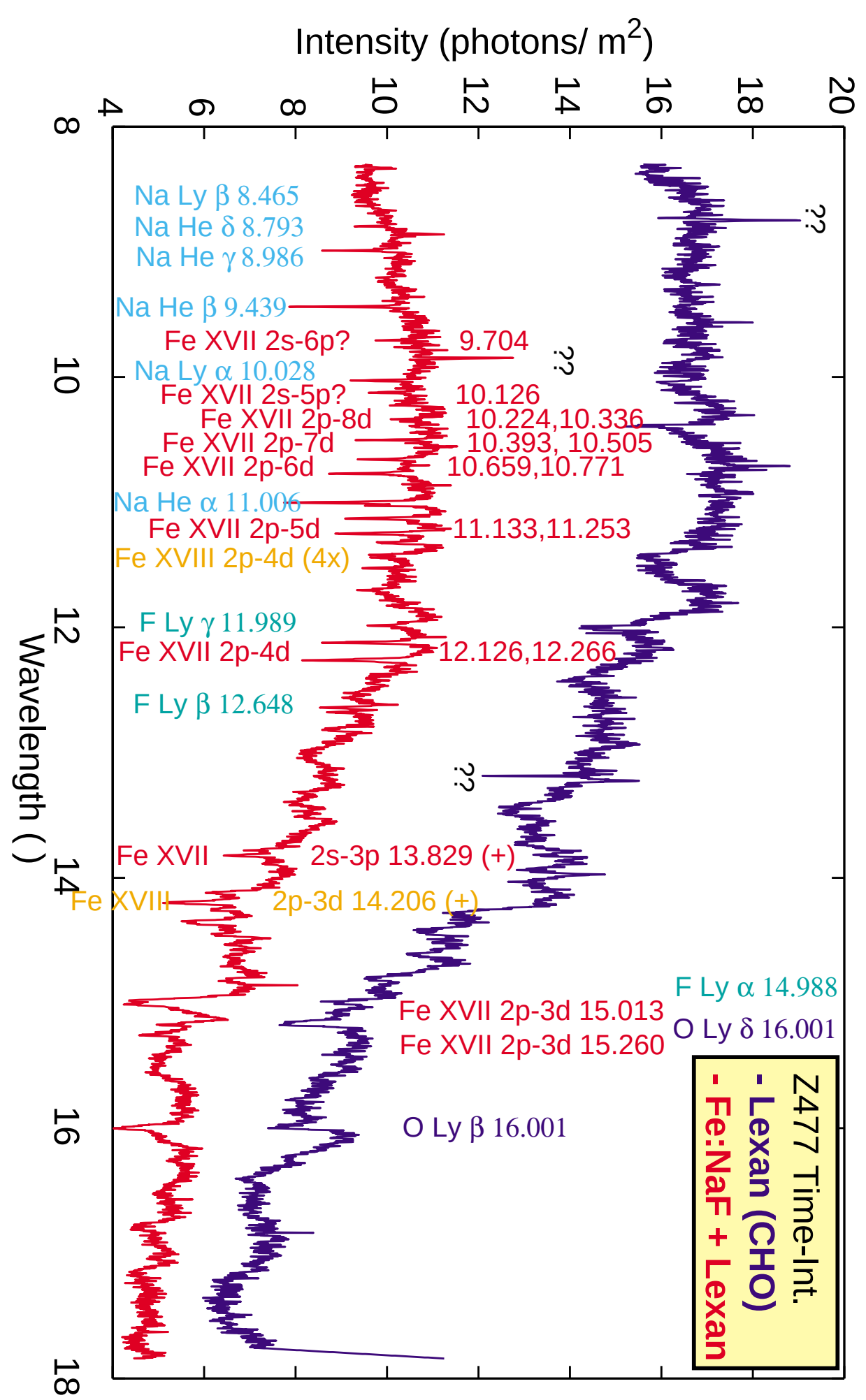
Intensity (photons/ m2)
4
6
8
10
12
14
16
18
20
Wavelength ( )
8
10
12
14
16
18
Na Ly β 8.465
Na He δ 8.793
Na He γ 8.986
Na He β 9.439
Fe XVII 2s-6p? 9.704
Na Ly α 10.028
Fe XVII 2s-5p? 10.126
Fe XVII 2p-8d 10.224,10.336
Fe XVII 2p-7d 10.393, 10.505
Fe XVII 2p-6d 10.659,10.771
Na He α 11.006
Fe XVII 2p-5d 11.133,11.253
Fe XVIII 2p-4d (4x)
F Ly γ 11.989
Fe XVII 2p-4d 12.126,12.266
F Ly β 12.648
Fe XVII 2s-3p 13.829 (+)
Fe XVIII 2p-3d 14.206 (+)
Fe XVII 2p-3d 15.013
Fe XVII 2p-3d 15.260
O Ly β 16.001
F Ly α 14.988
O Ly δ 16.001
??
??
??
Z477 Time-Int.
- Lexan (CHO)
- Fe:NaF + Lexan